Development of a strong field helicon plasma source

Shunjiro Shinohara[a] and Hiroshi Mizokoshi
Interdisciplinary Graduate School of Engineering Sciences, Kyushu University, Kasuga, Fukuoka 816-8580, Japan

(Received 17 November 2005; accepted 19 January 2006; published online 22 March 2006)

We developed a high-density helicon plasma source with a very strong field of up to 10 kG. Using a double-loop antenna wound around a quartz tube, 9.5 cm in inner diameter and 90 cm in axial length, initial plasmas with a high density more than 10^{13} cm^{-3} were successfully produced with a radio frequency power less than a few kilowatts, and with changing magnetic fields, fill pressures, and gas species. © *2006 American Institute of Physics.* [DOI: 10.1063/1.2173940]

Helicon wave plasma sources,[1–6] which have an excellent capability of producing current-free, high-density plasmas up to $>10^{13}$ cm^{-3} are thought to have promise for applications in various plasma fields such as plasma processing, fusion, and basic fields including the study of space plasmas and a magnetoplasma rocket.[7] A helicon wave scheme has the advantages of an easy operation and a wide range of operational parameters, e.g., the magnetic field due to nonresonant wave characteristics and the fill pressure. To further develop this source, it will be necessary to extend conventional parameter regimes such as the plasma size, e.g., very large[8–10] or small,[11,12] the applied magnetic field B, the excitation frequency f, e.g., higher frequency,[13] and the fill pressure, as well as novel ideas and technologies to control the plasma performance such as the density profile.[8,9]

According to a dispersion relationship of the helicon wave,[1–6] f lies between the ion and electron cyclotron frequencies, and the electron density is proportional to B if the parallel wave number is fixed. Therefore, it is important to increase B to apply a higher or a wider range of f and so achieve a higher density, which would facilitate a wider range of basic and application studies. For example, the excitation of the Alfvén wave in a smaller helicon source than what was possible before,[14] or in a much smaller helicon source than the dc discharge machine, the very large plasma device (LAPD),[15] could be realized. Furthermore, in a strong field a magnetized ion or even a magnetized dust experiment can be executed in a relatively small device. A strong field is also expected to contribute to the better plasma confinement across the field, which would lead to a more efficient plasma production. However, to our knowledge helicon discharges of more than 1.6 kG have not been realized,[16–19] and so helicon plasma performance above this field should be investigated to provide a basic database as well as to extend the conventional operational parameters. If our scheme has promise, in addition to the electromagnetic coil, a permanent magnet system that is being actively developed for the higher field region can be applied to ensure both compact size and simplicity.

To demonstrate the high field effect, we have developed a high-density helicon plasma source with a very strong field of up to 10 kG that are generated by a large coil current using iron yokes. Installing a double-loop antenna, initial plasmas with high densities more than 10^{13} cm^{-3} were successfully produced with a radio frequency (rf) power of less than a few kilowatts. Here, the plasma density as a function of the rf power, changing magnetic fields, fill pressure, and gas species is also briefly described. Our experiments are performed in a quartz discharge chamber with outer and inner diameters of 10 and 9.5 cm, respectively, and an axial length of 90 cm (see Figs. 1 and 2). The four main coils made by the NEC Tokin Corp. are 20 cm wide (horizontal direction) and 8.2 cm high (vertical direction), each with 160 turns of copper, and produce a uniform magnetic field in the central region: over 30 cm in the axial direction. At z (the vertical distance from the center) =23 cm this field becomes half of the central value at $z=0$ cm. This field is nearly constant along the radial direction; within the quartz's inner radius of 4.75 cm, it changes only by 0.2% at $z=0$ cm. Figure 3 shows a calculated contour map of the magnetic flux function along with vectors of B in the (x,z) space. Here, x is in the horizontal direction. These estimated fields using iron materials agree well with the ones in the measurements; the measured axial magnetic field increases almost linearly with the coil current of I_c, where the maximum current of $I_c=600$ A corresponds to the axial component of the magnetic field B of 9600 G.

Here, we have installed iron yokes (eight iron pillars, 5 cm in diameter) connected to the top and the bottom iron plates (yokes of 4 cm thickness) around the chamber (see Figs. 1–3). These iron materials can confine the outgoing field from the quartz chamber to increase the main field in the chamber area; without these materials, the estimated axial magnetic field at the center where $z=0$ cm is only about 60% of the one with the iron materials (present device), and there is a monotonic decreasing field along the z direction (at $z=35$ cm this field becomes half of the central value at $z=0$ cm). To change the magnetic field configurations without axial movements of the coils, each coil has four taps, which lead to normalized output currents of 0, 1/3, 2/3, and 1 (as units of the case of a full turn).

Next, the rf system, shown on the left of Fig. 2, is described. A double-loop antenna, which can excite the azimuthal mode number of $m=0$, is used as shown in the central part of Fig. 2. Two copper plates, 0.02 cm thick and 3 cm wide (vertical direction), are wound around the quartz tube

[a]Electronic mail: sinohara@aees.kyushu-u.ac.jp

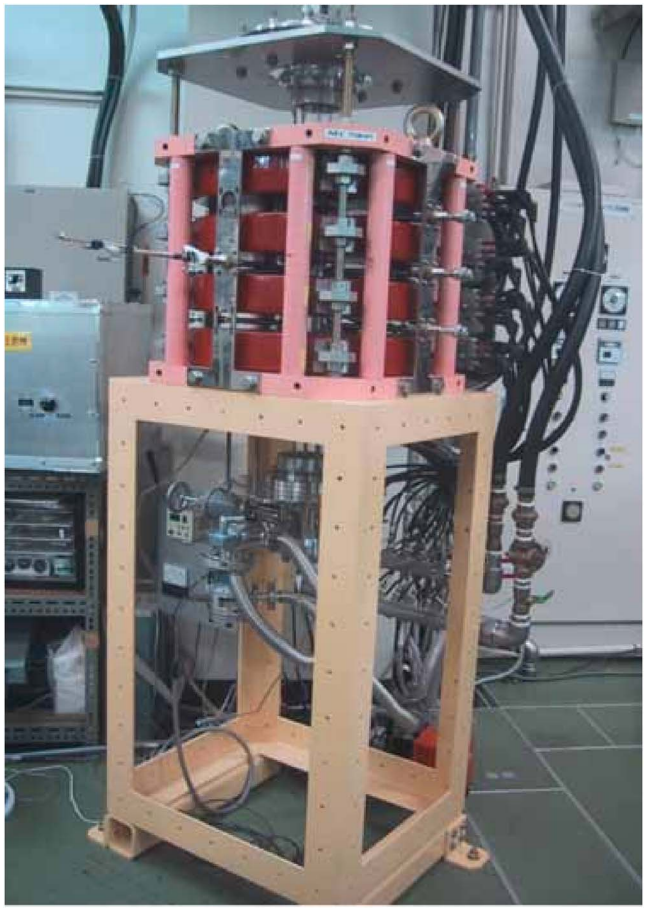

FIG. 1. (Color online) Photo of the strong field, high-density helicon plasma source.

with an axial gap of 6 cm. By changing the connection between the two loops, parallel and antiparallel rf current directions can be chosen. A parallel connection is used in most cases, considering a wider range of external operational parameters.[20] The antenna vacuum inductance and resistance (without plasma) are ~0.7 μH and ~0.8 Ω, respectively, including the feed lines from the matching box (partially seen on the middle left hand side of Fig. 1 and also on the left

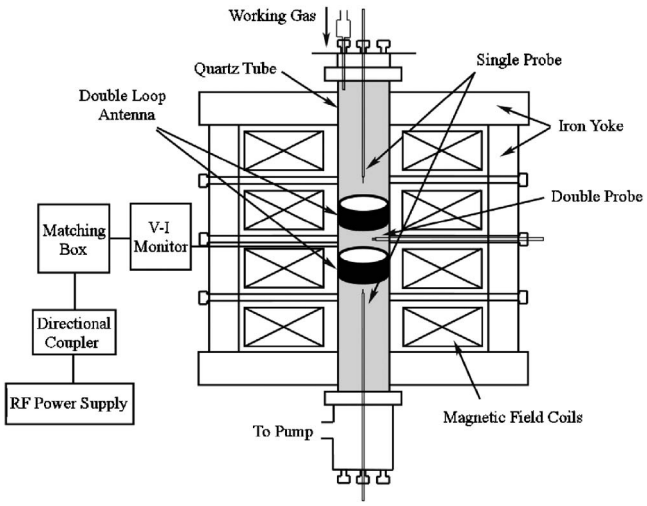

FIG. 2. Schematic view of the experimental setup.

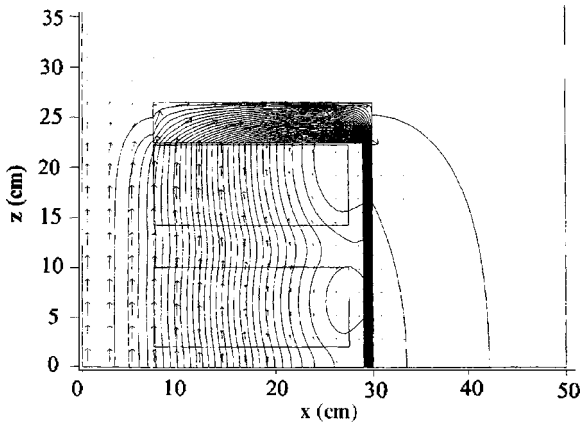

FIG. 3. Contour map of the magnetic flux function along with the calculated magnetic fields. Here, x and z are the horizontal (radial) and vertical directions, respectively.

hand side of Fig. 2) at $f=7$ MHz. In the matching box, a split tank circuit is employed, and forward and reflected rf powers, P_{for} and P_{ref}, respectively, are monitored using a directional coupler [G3438 (Werlatone Inc.)]. The rf input power P_{inp} to the plasma source is defined as $P_{\text{inc}}-P_{\text{ref}}$. The antenna rf current and rf voltage are measured by the handmade current and voltage monitors, which are calibrated under a low rf power operation. In our experiments, the maximum output power of the rf amplifier [CF-0505-3/15 (Pearl Kogyo Co., Ltd.)] is 5 kW. To reduce heat damage to the rf coils and probes, a pulsed mode (typical pulse width is 9 ms with a duty cycle of 0.075) operation is employed.

Using a small turbomolecular pump at a pumping speed of 50 l/s (on the bottom side of the chamber in Figs. 1 and 2), the base pressure of our device is less than several times 10^{-6} Torr. The working gas coming through a needle valve (the top side of the chamber in Figs. 1 and 2) is argon (Ar), unless specified, with a fill pressure, P_{Ar}, of 1–50 mTorr. The spatial plasma parameters, such as electron density n_e and electron temperature T_e (typically 3–5 eV), are measured by scanning Langmuir probes (shown in Fig. 2). Data were stored in a data logger [DL2300AP (NEC San-ei Instruments, Ltd.)] with a maximum sampling rate of 10 μs and data of 16 bits. Ordinary digital cameras are used to monitor the plasma light.

Figure 4 shows an example of n_e as a function of P_{inp} with $P_{\text{Ar}}=10$ mTorr, changing B. Here, n_e, measured at the axis center of $x=z=0$ cm, is derived from the ion saturation current I_{is}, assuming $T_e=4$ eV, and I_{is} is taken during a period of steady state at the later stages of the discharge. From this figure, with P_{inp} less than 1 kW, a density jump to the order of 10^{13} cm^{-3}, known as a mode change from inductively coupled plasma[21] (ICP) to helicon plasma discharges,[22] is observed. In the case of a lower field ($<$2000 G), the density jump (simultaneously, a 2–3.5 times jump in the antenna resistances is experienced) is clearer, and the density increment in this jump is larger compared to that in the case of the higher field. On the other hand, before the density jump, n_e is higher in the high field than in the low field. The threshold power for the density jump P_{th} is lower in the high field as long as a clear density jump is observed ($B<2000$ G), which is opposite to the result[23] previously reported using a smaller tube of 5 cm in diameter but with a

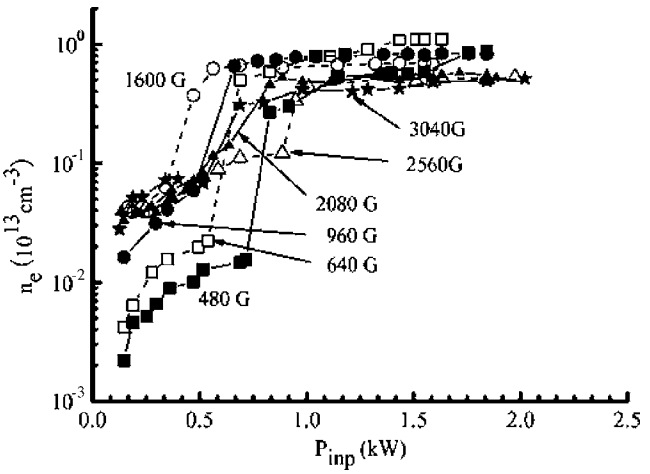

FIG. 4. Relationship between n_e and P_{inp} for various B with P_{Ar} =10 mTorr.

higher pressure of P_{Ar}=51 mTorr: P_{th} is lower in the lower field.

In this figure, the dependence of n_e on B after the jump shows that n_e becomes higher with B (from 480 to 640 G), and then decreases gradually with B (not shown). In the cases of B=480 and 640 G, the density roughly agrees with that expected from the dispersion relation of n_e (10^{13} cm^{-3}) $\sim 0.0014B$ (G) using an excited wavelength of 46 cm, which is the same as the uniform B region in our device. However, above $B \sim 1000$ G, the density obtained reaches well below this expected value, and there is a tendency for relative density fluctuation (antenna resistance) increases (decreases) with B. This discrepancy may be related, for example, to the lack of input power coming from the shorter effective axial size due to the poor confinement along the axis[24] or to the enhancement of the instabilities,[18] both of which should be subjected to further studies.

With respect to production efficiency, N_e/P_{inp} is $\sim$0.5 in units of 10^{13} cm^{-3}/W in the case of B=640 G after the density jump, where N_e is the total number of electrons. The obtained ratio is four to five times smaller than the scaling,[25] where N_e/P_{inp} is roughly proportional to a^2 (a: plasma radius), using a model of the cross field diffusion of ions derived from conditions of longer axial plasma size and smaller plasma radius without a strong magnetic field. The lower value of N_e/P_{inp} is the result of the shorter axial plasma size (dominant loss along the field): a short axial size of 10 cm with a 4.5 cm diameter tube[24] shows a smaller value of N_e/P_{inp} that is less than 1/10 of the expected scaling.[25] By shortening the axial plasma size using a spiral antenna with a large diameter chamber,[8,9] N_e/P_{inp} also becomes lower.[26]

A similar relationship between n_e and P_{inp}, as in Fig. 4, is observed, changing P_{Ar}: 1.8 and 20 mTorr, as shown in Fig. 5. The high-pressure case of 20 mTorr shows a greater increment of n_e at the density jump than in the low field case, while the high field case at both pressures of 1.8 and 20 mTorr (up to 4000 G) shows a gradual increase in n_e with P_{inp} without any clear jumps. This indicates the ICP discharge and that a greater input power may be necessary to facilitate jumps; again, this should be the focus of a future study. With a constant P_{inp} after the density jump, n_e becomes higher and its relative fluctuation is lower with the increase in P_{Ar}; however, the ionization degree η decreases

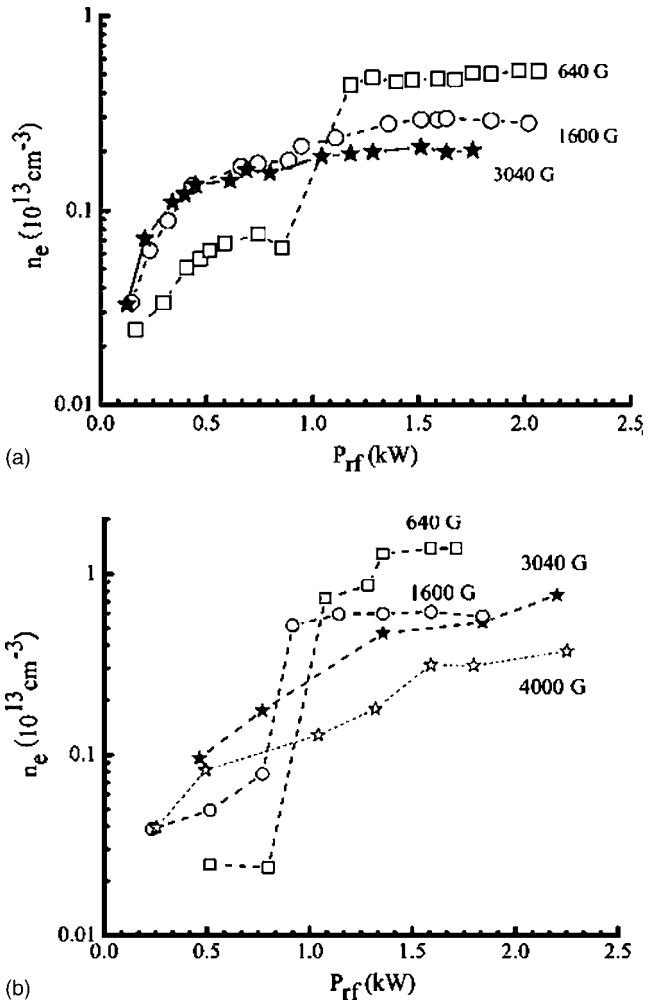

FIG. 5. Relationship between n_e and P_{inp} for various B with P_{Ar}=(a) 1.8 and (b) 20 mTorr.

with P_{Ar}; e.g., in the case of P_{inp}=1.6 kW and B=640 G, n_e and η are $0.5(1.6)\times 10^{13}$ cm^{-3} and 8 (1.5)%, respectively, with P_{Ar}=1.4(33) mTorr.

rf plasma discharges using other gas species instead of argon have been undertaken. Xe (He) plasma shows a higher (lower) density with the same external conditions. With P_{Xe} (Xe gas pressure) =10 mTorr and B=1360 G, the density jumps at $P_{\mathrm{th}} \sim 0.4$ kW from $\sim 7\times 10^{11}$ to $\sim 2\times 10^{13}$ cm^{-3}. On the other hand, He plasma shows almost a linear increase in density with increasing power with an offset power of $\sim$0.2 kW, i.e., $n_e \sim 3.5\times 10^{10}$ (2.5×10^{11}) cm^{-3} with P_{inp} =0.4 (1.5) kW, under conditions of He gas pressure P_{He} =10 mTorr and B=480 G. These features are consistent with previous results.[8,18,19,27] Similar to Ar discharges, n_e increases with B, then decreases with B above a certain critical magnetic field B_{cr} in He and Xe discharges. It is still an open question whether B_{cr} is close to the field that satisfies a lower hybrid frequency.[16–19,28,29]

The authors would like to thank Professor Y. Kawai for his continuous encouragement. The research has been partially supported by Grants-in-Aid for Scientific Research (B)(2), Nos. 15340199 and 14350514, and (A)(2), No. 17206084, from the Japan Society for the Promotion of Science.

[1] R. W. Boswell, Phys. Lett. **33A**, 457 (1970).
[2] M. A. Lieberman and A. J. Lichtenberg, *Principles of Plasma Discharges and Materials Processing* (Wiley, New York, 1994).
[3] S. Shinohara, Jpn. J. Appl. Phys., Part 1 **36**, 4695 (1997), and references therein.
[4] R. W. Boswell and F. F. Chen, IEEE Trans. Plasma Sci. **25**, 1229 (1997), and references therein.
[5] F. F. Chen and R. W. Boswell, IEEE Trans. Plasma Sci. **25**, 1245 (1997), and references therein.
[6] S. Shinohara, J. Plasma Fusion Res. **78**, 5 (2002), and references therein (mostly in Japanese).
[7] F. R. Chang-Díaz, Trans. Fusion Technol. **35**, 87 (1999).
[8] S. Shinohara and T. Tanikawa, Rev. Sci. Instrum. **75**, 1941 (2004).
[9] S. Shinohara and T. Tanikawa, Phys. Plasmas **12**, 044502 (2005).
[10] B. P. Cluggish *et al.*, Phys. Plasmas **12**, 057101 (2005).
[11] M. Nisoa, Y. Sakawa, and T. Shoji, Jpn. J. Appl. Phys., Part 2 **38**, L777 (1999).
[12] K. Toki, S. Shinohara, T. Tanikawa, and K. P. Shamrai, Thin Solid Films (in press).
[13] Y. Sakawa, H. Kunimatsu, H. Kikuchi, and T. Shoji, Phys. Plasmas **11**, 286 (2004).
[14] M. J. Hanna and C. Watts, Phys. Plasmas **8**, 4251 (2001).
[15] W. Gekkelman, H. Pfister, Z. Lucky, J. Bamber, D. Leneman, and J. M. Maggs, Rev. Sci. Instrum. **62**, 2875 (1991).
[16] P. Zhu and R. W. Boswell, Phys. Rev. Lett. **63**, 2805 (1989).
[17] P. Zhu and R. W. Boswell, Phys. Fluids B **3**, 869 (1991).
[18] M. Light, F. F. Chen, and P. K. Colestock, Phys. Plasmas **8**, 4675 (2001).
[19] Y. Sakawa, T. Takino, and T. Shoji, Phys. Plasmas **6**, 4759 (1999).
[20] S. Shinohara, N. Kaneda, and Y. Kawai, Thin Solid Films **316**, 139 (1998).
[21] J. Hopwood, Plasma Sources Sci. Technol. **1**, 109 (1992).
[22] A. R. Ellingboe and R. W. Boswell, Phys. Plasmas **3**, 2797 (1996).
[23] S. Shinohara and K. Yonekura, Plasma Phys. Controlled Fusion **42**, 41 (2000).
[24] M. Nisoa, Y. Sakawa, and T. Shoji, Jpn. J. Appl. Phys., Part 2 **38**, L777 (1999).
[25] T. Tanikawa and S. Shinohara, *Proceedings of the International Congress on Plasma Physics*, (International Advisory Committee, Nice, 2004) (http://hal.ccsd.cnrs.fr/ccsd-00002013).
[26] T. Tanikawa, S. Shinohara, and K. Toki, *Proceedings of the 56th International Astronautical* Congress (International Astronautical Federation, Fukuoka, 2005), Paper IAC-05-C4.4.05.
[27] T. Tanikawa and S. Shinohara, Thin Solid Films (in press).
[28] S. M. Yun, J. H. Kim, and H. Y. Chang, J. Vac. Sci. Technol. A **15**, 673 (1997).
[29] S. M. Yun and H. Y. Chang, Phys. Lett. A **248**, 400 (1998).